# Orbital-angular-momentum mode-group multiplexed transmission over a graded-index ring-core fiber based on receive diversity and maximal ratio combining

**JUNWEI ZHANG,[1†] GUOXUAN ZHU,[1†] JIE LIU,[1,*] XIONG WU,[1] JIANGBO ZHU,[2] CHENG DU,[3] WENYONG LUO,[3] YUJIE CHEN,[1] AND SIYUAN YU[1,2]**

[1]*State Key Laboratory of Optoelectronic Materials and Technologies, School of Electronics and Information Technology, Sun Yat-Sen University, Guangzhou 510006, China*
[2]*Photonics Group, Merchant Venturers School of Engineering, University of Bristol, Bristol BS8 1UB, UK*
[3]*Fiberhome Telecommunication Technologies Co. Ltd,Wuhan, 430074, China*
[†]*These authors contributed equally to this work.*
**liujie47@mail.sysu.edu.cn*

**Abstract**: An orbital-angular-momentum (OAM) mode-group multiplexing (MGM) scheme using high-order mode groups (MGs) in a graded-index ring-core fiber (GIRCF) is proposed, in which a receive-diversity architecture is designed for each MG to suppress the mode partition noise resulting from random intra-group mode crosstalk. The signal-to-noise ratio (SNR) of the received signals is further improved by a simple maximal ratio combining (MRC) technique on the receiver side to efficiently take advantage of the diversity gain of the receiver. Intensity-modulated direct-detection (IM-DD) systems transmitting three OAM mode groups with total 100-Gb/s discrete multi-tone (DMT) signals over a 1-km GIRCF and two OAM mode groups with total 40-Gb/s DMT signals over an 18.4-km GIRCF are experimentally demonstrated, respectively, to confirm the feasibility of our proposed OAM-MGM scheme.



**OCIS codes:** (060.2330) Fiber Optics Communications; (060.2270) Fiber characterization; (060.4230) Multiplexing.

## References and links

1. D. J. Richardson, J. M. Fini, and L. E. Nelson, "Space-division multiplexing in optical fibres," Nat. Photonics **7**(5), 354–362 (2013).
2. N. K. Fontaine, R. Ryf, H. Chen, A. V. Benitez, B. Guan, R. Scott, B. Ercan, S. J. B. Yoo, L. E. Grüner-Nielsen, Y. Sun, R. Lingle, E. Antonio-Lopez, and R. Amezcua-Correa, "30×30 MIMO Transmission over 15 Spatial Modes," in Optical Fiber Communication Conference Post Deadline Papers, OSA Technical Digest (online) (Optical Society of America, 2015), paper Th5C.1.
3. S. Randel, R. Ryf, A. Sierra, P. J. Winzer, A. H. Gnauck, C. A. Bolle, R. J. Essiambre, D. W. Peckham, A. McCurdy, and R. Lingle, "6× 56-Gb/s mode-division multiplexed transmission over 33-km few-mode fiber enabled by 6× 6 MIMO equalization," Opt. Express **19**(17), 16697–16707 (2011).
4. S. O. Arik, K.-P. Ho, and J. M. Kahn, "Optical network scaling: roles of spectral and spatial aggregation," Opt. Express **22**(24), 29868–29887 (2014).
5. P. J. Winzer, "Making spatial multiplexing a reality," Nat. Photonics **8**, 345–348 (2014).
6. S. O. Arik, K.-P. Ho, and J. M. Kahn, "Group Delay Management and Multiinput Multioutput Signal Processing in Mode-Division Multiplexing Systems," J. Lightwave Technol. **34**(11), 2867–2880 (2016).
7. K.-P. Ho and J. M. Kahn, "Statistics of group delays in multimode fiber with strong mode coupling," J. Lightwave Technol. **29**(21), 3119–3128 (2011).
8. K. Zhong, X. Zhou, T. Gui, L. Tao, Y. Gao, W. Chen, J. Man, L. Zeng, A. P. T. Lau, and C. Lu, "Experimental study of PAM-4, CAP-16, and DMT for 100 Gb/s short reach optical transmission systems," Opt. Express **23**(2), 1176–1189 (2015).
9. E. Ip, G. Milione, M. J. Li, N. Cvijetic, K. Kanonakis, J. Stone, G. Peng, X. Prieto, C. Montero, V. Moreno, and J. Liñares, "SDM transmission of real-time 10GbE traffic using commercial SFP + transceivers over 0.5km elliptical-core few-mode fiber," Opt. Express **23**(13), 17120–17126 (2015).
10. K. Ingerslev, P. Gregg, M. Galili, F. D. Ros, H. Hu, F. Bao, M. A. U. Castaneda, P. Kristensen, A. Rubano, L. Marrucci, S. Ramachandran, K. K. Rottwitt, T. Morioka, and L. K. Oxenlowe, "12 Mode, MIMO-free OAM

transmission," in Optical Fiber Communication Conference, OSA Technical Digest (online) (Optical Society of America, 2017), paper M2D.1.
11. B. Franz, and H. Bülow, "Mode Group Division Multiplexing in Graded‐Index Multimode Fibers," Bell Labs Technical Journal **18**, 153–172 (2013).
12. H. Liu, H. Wen, J. C. A. Zacarias, J. Antonio-Lopez, N. Wang, P. Sillard, A. Amezcua-Correa, R. A. Correa, and G. Li, "3x10 Gb/s mode group-multiplexed transmission over a 20 km few-mode fiber using photonic lanterns," in Optical Fiber Communication Conference, OSA Technical Digest (online) (Optical Society of America, 2017), paper M2D.5.
13. G. Labroille, P. Jian, L. Garcia, J.-B. Trinel, R. Kassi, L. Bigot, J.-F. Morizur , "30 Gbit/s Transmission over 1 km of Conventional Multimode Fiber using Mode Group Multiplexing with OOK modulation and direct detection," in Optical Communication (ECOC), 2015 European Conference on IEEE 2015, pp. 1–3.
14. C. Simonneau, A. D'amato, P. Jian, G. Labroille, J.-F. Morizur, and G. Charlet, "4x50Gb/s transmission over 4.4 km of multimode OM2 fiber with direct detection using mode group multiplexing," in Optical Fiber Communication Conference, OSA Technical Digest (online) (Optical Society of America, 2016), paper Tu2J. 3.
15. K. Benyahya, C. Simonneau, A. Ghazisaeidi, N. Barré, P. Jian, J. Morizur, G. Labroille, M. Bigot, P. Sillard, J. G. Provost, H. Debrégeas, J. Renaudier, and G. Charlet, "Multiterabit Transmission over OM2 Multimode Fiber with Wavelength and Mode Group Multiplexing and Direct Detection," Journal of Lightwave Technology (2017).
16. F. Feng, X. Guo, G. S. Gordon, X. Jin, F. Payne, Y. Jung, Q. Kang, S. Alam, P. Barua, J. Sahu, D. Richardson, I. H. White, and T. D. Wilkinson, "All-optical Mode-Group Division Multiplexing Over a Graded-Index Ring-Core Fiber with Single Radial Mode," in Optical Fiber Communication Conference, OSA Technical Digest (online) (Optical Society of America, 2016), paper W3D.5.
17. F. Feng, X. Jin, D. O'Brien, F. P. Payne, and T. D. Wilkinson, "Mode-Group Multiplexed Transmission using OAM modes over 1 km Ring-Core Fiber without MIMO Processing," in Optical Fiber Communication Conference, OSA Technical Digest (online) (Optical Society of America, 2017), paper Th2A.43.
18. F. Feng, Y. Jung, H. Zhou, R. Zhang, S. Chen, H. Wang, Y. Yang, S. U. Alam, D. J. Richardson, and Timothy D. Wilkinson, "High-Order Mode-Group Multiplexed Transmission over a 24km Ring-Core Fibre with OOK Modulation and Direct Detection," in Optical Communication (ECOC), 2017 European Conference on IEEE 2017, pp. 1–3.
19. X. Jin, A. Gomez, K. Shi, B. C. Thomsen, F. Feng, G. S. D. Gordon, T. D. Wilkinson, Y. Jung, Q. Kang, P. Barua, J. Sahu, S. Alam, D. J. Richardson, D. C. O'Brien, and F. P. Payne, "Mode Coupling Effects in Ring-Core Fibers for Space-Division Multiplexing Systems," J. Lightwave Technol. **34**(14), 3365–3372 (2016).
20. Z. Guo, J. Zhu, X. Wu, J. Liu, C. Du, H. Yan, Z. Hu, X. Wang, Y. Chen, W. Luo, S. Li, X. Zheng, X. Cai and S. Yu, "Scalable Orbital Angular Momentum Mode Division Multiplexing Transmission over 10km Graded-index Ring-core Fiber," in Optical Communication (ECOC), 2017 European Conference on IEEE 2017, pp. 1–3.
21. H. Huang, G. Milione, M. P. Lavery, G. Xie, Y. Ren, Y. Cao, N. Ahmed, T. An Nguyen, D. A. Nolan, M.-J. Li, M. Tur, R. R. Alfano, and A. E. Willner, "Mode division multiplexing using an orbital angular momentum mode sorter and MIMO-DSP over a graded-index few-mode optical fibre," Sci. Rep. **5**, 14931 (2015).
22. S. Kawakami, and M. Ikeda, "Transmission Characteristics of a Two-Mode Optical Waveguide," IEEE J. of Quantum Electronics **14**(8), 608–614(1978). J. Zhang, Y. Zheng, X. Hong, and C. Guo, "Increase in Capacity of an IM/DD OFDM-PON Using Super-Nyquist Image Induced Aliasing and Simplified Nonlinear Equalization," J. Lightwave Technol. **35**(19), 4105–4113 (2017).
23. J. R. Barry, E. A. Lee, D. G. Messerschmitt, Digital communication, Springer Science & Business Media, 2012.
24. J. Zhang, Y. Zheng, X. Hong, and C. Guo, "Increase in Capacity of an IM/DD OFDM-PON Using Super-Nyquist Image Induced Aliasing and Simplified Nonlinear Equalization," J. Lightwave Technol. 35(19), 4105–4113 (2017).
25. S. O. Arik, D. Askarov, and J. M. Kahn, "Effect of mode coupling on signal processing complexity in mode-division multiplexing," J. Lightwave Technol. **31**(3), 423–431 (2013).
26. C.Brunet, B. Ung, L. Wang, Y. Messaddeq, S. LaRochelle, and L. A. Rusch," Design of a family of ring-core fibers for OAM transmission studies," Opt. Express **23**, 10553–10563 (2015).
27. S. Ramachandran, P. Gregg, P. Kristensen, and S. E. Golowich, "On the scalability of ring fiber designs for OAM multiplexing," Opt. Express **23**, 3721–3730 (2015).
28. Yong Soo Cho, Jaekwon Kim, Won Young Yang, Chung-Gu Kang,MIMO-OFDM Wireless Communication with MATLAB, John Wiley &Sons (Asia), Singapore, 2010.
29. D. Marcuse, "Microdeformation losses of single-mode fibers," Appl. Opt. **23**, 1082 (1984).
30. Z. Zhang, J. Gan, X. Heng, Y. Wu, Q. Li, Q. Qian, D. Chen, and Z. Yang, "Optical fiber design with orbital angular momentum light purity higher than 99.9," Opt. Express 23(23), 29331–29341 (2015).
31. W. Wang, Y. Li, Z. Y. Guo, R. Z. Li, J. R. Zhang, A. J. Zhang, and S. L. Qu, "Ultra-thin optical vortex phase plate based on the metasurface and the angular momentum transformation," J. Opt. **17**(4), 045102 (2015).

## 1. Introduction

Space-division multiplexing (SDM) in optical fiber has recently been intensively investigated, aiming for solving the current single mode fiber (SMF) capacity crunch by utilizing the spatial or mode domain of light [1]. Among various SDM schemes, mode-division

multiplexing (MDM) techniques based on multi-mode fibers (MMFs) or few-mode fibers (FMFs) can increase the number of transmission channels within a limited aperture and thus increase the capacity density of a single fiber core [2–4]. In addition, the design of amplifiers, switches and other inline components in MDM schemes can be highly compact, which makes the scaling of optical networks more cost effective and energy efficient [4,5]. The main limitations of MMF-based MDM systems are the crosstalk and distortion resulting from mode coupling and modal dispersion during fiber transmission. In long-haul MDM systems, crosstalk between all mode pairs is non-negligible [6]. As a result, adaptive full-size multiple-input multiple-output (MIMO) equalization is required, in which case the fiber in the strong-mode-coupling regime is more desirable to decrease the differential group delay (DGD) and thus reduce the complexity of MIMO processing in these systems [7]. On the other hand, in short-reach applications (e.g. intra-data-center network, local area network, access network, etc.), intensity-modulated direct-detection (IM-DD) schemes without MIMO processing are preferred, considering the system cost and power consumption [8]. Weakly coupled MDM scheme can be considered as one of the promising solutions to increase the capacity of short-reach transmission systems, since modal crosstalk and dispersion can be neglected for short-reach transmission and the need of coherent optical detection and MIMO processing can thus be eliminated [9,10]. However, reducing mode coupling among all the fiber modes, especially the (quasi-)degenerate modes, over > 2-km fiber distance still remains a challenge in these schemes.

Given the increasing mode coupling in MMFs over distance, mode-group multiplexing (MGM) [11] emerges as an alternative approach for MIMO-free MMF transmission, in which (quasi-) degenerate modes within each mode group (MG) are regarded as one data channel. The weak-coupling among different MGs can be exploited to eliminate the need of coherent detection and MIMO processing at the receivers. Several MGM schemes have been implemented based on conventional MMFs or FMFs, in which all the intra-group modes need to be detected simultaneously at the receiver to avoid the mode partition noise resulting from the random intra-group mode crosstalk [12–14]. However, as the number of intra-group modes in graded-index (GI) MMFs linearly increases with the MG order [as shown in Fig. 1(a)], reception of high-order MGs will become increasingly complex, when mode demultiplexer that demultiplexes all intra-group modes is utilized. The MG (de)multiplexer [15] can help address this issue. However, relatively higher crosstalk between adjacent higher-order MGs in the MG (de)multiplexer and optical fibers limits scalability of the MMF-based MGM systems to high-order MGs.

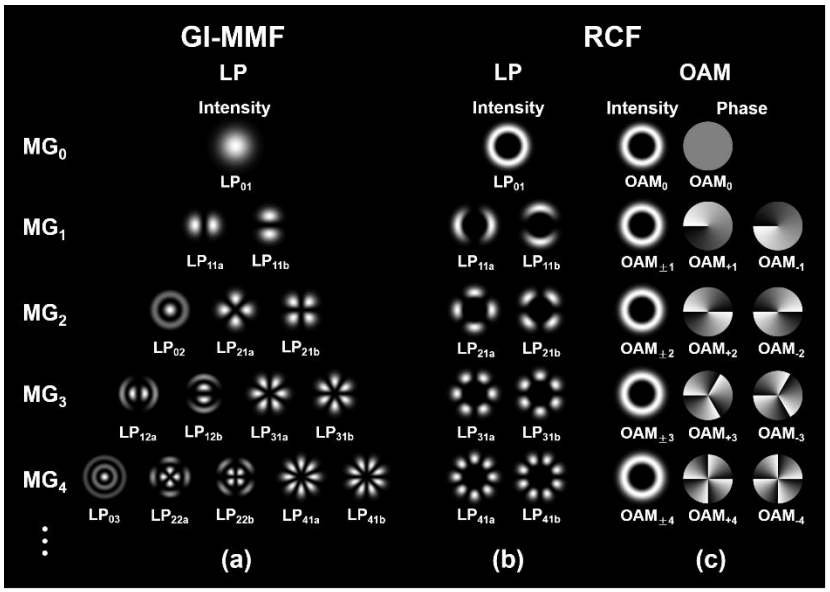


Fig. 1. Diagrams of (a) intensity of the linearly polarized (LP) modes in each mode group (MG) of the GI-MMF; (b) intensity of the LP modes in each MG of the ring-core fiber (RCF); (c) intensity and phase of the OAM modes in each MG of the RCF. Here note that each fiber mode shown in this figure can be further subdivided into two modes with orthogonal polarizations.

Ring-core-fiber (RCF) based MGM systems have been reported recently [16–18]. With the ring-core profile allowing for only single-radial-order modes, a fixed number of near-degenerate modes are supported by the RCFs for each high-order MG [as shown in Figs. 1(b) and 1(c)], for which modular reception for each high-order MG can be more easily implemented. In addition, the coupling strength between adjacent MGs of the RCFs decreases significantly with the increasing azimuthal mode order [19]. These characteristics provide RCFs with a higher scalability in the optical mode space. Both the linearly polarized (LP) and orbital angular momentum (OAM) mode basis can be utilized for MGM in RCFs. MG (de)multiplexing of the RCF-based MGM schemes that have been reported is mainly based on weighted composite phase masks, in which the relative amplitude and phase of all intra-group modes should be measured at the receiving end [16–18]. However, as the relative amplitude and phase of the intra-group modes change randomly during fiber transmission, adaptive measurement or evaluation of the amplitude and phase distribution of degenerate modes in optical domain may be quite difficult in practical implementations.

Therefore, in this paper, an OAM-MGM system utilizing high-order MGs in a graded-index ring-core fiber (GIRCF) base on a receive-diversity scheme is proposed. In the receive-diversity scheme, a single-input two-output architecture is designed for each MG channel and simple digital signal processing (DSP) is employed to adaptively equalize the mode partition noise induce by random intra-group mode crosstalk. MIMO processing is not required in the proposed scheme. Moreover, a simple maximal ratio combining (MRC) technique can be utilized at the receiver of this scheme to efficiently take advantage of the diversity gain of receiver and improve the signal-to-noise ratio (SNR) of the received signals. In order to prove the feasibility of the proposed OAM-MGM scheme, two sets of intensity-modulated direct-detection (IM-DD) systems are implemented experimentally: a system transmitting three OAM MGs with a total of 100-Gb/s discrete multi-tone (DMT) signals over a 1-km GIRCF, and a system transmitting two OAM MGs with a total of 40-Gb/s DMT signals over an 18.4-km GIRCF. The measured results show that by using the receive-diversity architecture and MRC technique, there will be an average of ~3 dB improvement of

receiving sensitivity at the BER of $3.8\times10^{-3}$ for both of the OAM-MGM systems over 1-km and 18.4-km GIRCF, compared with that in the OAM-MGM system based on single-PD detection. In addition, when the receive-diversity architecture is utilized, MRC-based system performance is superior to that of the system with equal ratio combining (ERC), especially in the case that there is a great difference of BER performance between the two received branches.

## 2. Proposed OAM-MGM scheme

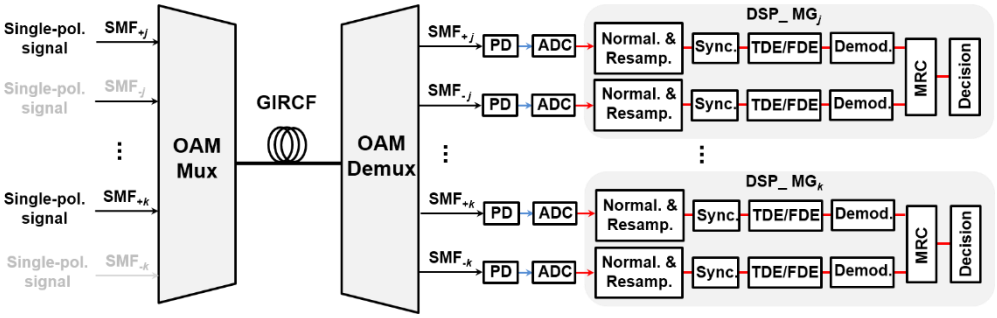


Fig. 2. Block diagram of the proposed OAM mode-group (de)multiplexing scheme. $SMF_i$: the single mode fiber input/output port for the $i_{th}$ OAM modes; $MG_i$: the $i_{th}$ OAM mode group including OAM modes $<\pm i, \pm s>$ ($i \in \{j, j+1,\ldots, k\}$ in which $k$ and $j$ are integers, and $k > j > 0$; $\pm i$ being the azimuthal mode order and $\pm s$ being the left- or right-hand circular polarizations); Normal.: Normalization; Resamp.: resampling; demod.: demodulation.

The block diagram of the proposed OAM-MGM scheme is shown in Fig. 2. For each high-order (MG order > 0) MG, optical carrier at a fixed wavelength is intensity modulated by an electrical signal to generate the optical signal at the transmitter. Considering the linear or quasi-linear relationship between the light intensity and the electrical signal, the electric field of the intensity modulated optical signal for the $i_{th}$ MG can be expressed as:

$$E_i(t) = A_i\sqrt{\alpha_i[V_{i0} + V_i(t)]}e^{j(\omega_0 t+\varphi_i)} \tag{1}$$

where $A_i$, $\omega_0$ and $\varphi_i$ denote the amplitude, frequency and phase of the optical carrier, respectively, while $\alpha_i$ is the ratio between optical powers before and after electro-optic modulation at the transmitter of $i_{th}$ MG and here can be considered as a constant. $V_{i0}$ and $V_i(t)$ refer to the DC and AC components of the electrical signal carried by the $i_{th}$ MG channel, respectively. The generated optical signals of all MGs are launched to their respective SMF input ports of the OAM multiplexer. Here note that, for each OAM MG that includes four degenerate OAM modes $<\pm i, \pm s>$ ($\pm s$ being the left- or right-hand circular polarizations and $\pm i$ being the azimuthal mode order) [20], only one OAM mode is excited at the transmitter, as shown in Fig. 2. Then the optical signals are OAM mode converted and multiplexed with an OAM multiplexer (OAM mux, e.g. the OAM mode sorter [21]), and finally coupled into the GIRCF. Since the GIRCF here is designed with large inter-group effective index differences but very small effective index differences between intra-group modes [20], random intra-group mode crosstalk resulting from strong modal coupling is inevitable during fiber transmission, while there is only low inter-MG coupling. As a result, all the four intra-group modes should be simultaneously detected at the receiver to avoid the mode partition noise [13], while small power loss due to weak coupling between MGs, which is proportional to the fiber length and does not vary with time [22], can be neglected. The electric field of the four degenerate modes in the $i_{th}$ MG after a certain–distance GIRCF transmission can be expressed as:

$$E_{\mathrm{OAM}_{l,m}}(t) = A'_{l,m}(t)\sqrt{\alpha_i[V_{i0}+V_i(t)]}e^{j(\omega_0 t+\varphi'_{l,m}(t))}e^{jl\theta} \tag{2}$$

where $l$ equals to $\pm i$ (the azimuthal mode order) and $m$ equals to $\pm s$ (the left- or right-hand circular polarizations). $A'_{l,m}(t)$ and $\varphi'_{l,m}(t)$ denote the amplitude and phase of the $\mathrm{OAM}_{l,m}$ mode, respectively, whose values randomly change in time because of random crosstalk between intra-group modes. $\theta$ is the azimuthal angle. As power loss of the $i_{th}$ MG resulting from fiber loss and inter-group crosstalk is related to the fiber length, given a certain fiber structure and length, the total optical power of all the four modes of the $i_{th}$ MG can be given by the following expression:

$$\begin{aligned} P_{\mathrm{MG}_i}(t) &= \sum_{l=\pm i}\sum_{m=\pm s}\left|E_{\mathrm{OAM}_{l,m}}(t)\right|^2 \\ &= \alpha_i[V_{i0}+V_i(t)]\sum_{l=\pm i}\sum_{m=\pm s}\left|A'_{l,m}(t)\right|^2 = C\alpha_i[V_{i0}+V_i(t)] \end{aligned} \tag{3}$$

where $C = \sum_{l=\pm i}\sum_{m=\pm s}\left|A'_{l,m}(t)\right|^2$ is a constant. As a result, the total optical power of the $i_{th}$ MG is proportional to the electrical signal, which theoretically proves that the mode partition noise due to random modal crosstalk can be eliminated when all the four intra-group modes are simultaneously power detected.

After mode-converted and demultiplexed by the OAM demultiplexer (OAM demux), polarization multiplexed fundamental modes at each SMF output port of the OAM demux, which are converted from the two OAM modes with the same azimuthal mode order but orthogonal polarizations, respectively, are detected by one photo detector (PD). Considering the different power response of the two received branches and regardless of the noise and bandwidth limitation of PD, the detected photo current after square-law detection of the $i_{th}$ MG is

$$\begin{aligned} I_{\mathrm{MG}_i}(t) &= \mu_{+i}\sum_{m=\pm s}\left|E_{\mathrm{OAM}_{+i,m}}(t)+n_{\mathrm{OAM}_{+i,m}}(t)\right|^2 + \mu_{-i}\sum_{m=\pm s}\left|E_{\mathrm{OAM}_{-i,m}}(t)+n_{\mathrm{OAM}_{-i,m}}(t)\right|^2 \\ &= \alpha_i[V_{i0}+V_i(t)](\mu_{+i}\sum_{m=\pm s}\left|A'_{+i,m}(t)\right|^2 + \mu_{-i}\sum_{m=\pm s}\left|A'_{-i,m}(t)\right|^2) + I_n(t) \end{aligned} \tag{4}$$

where $\mu_{+i}$ and $\mu_{-i}$ are responsivity of the two received branches, respectively, considering power response of both the optical transmission paths and PDs. $n_{\mathrm{OAM}_{\pm i,\pm s}}(t)$ refer to the amplified spontaneous emission (ASE) noise after optical filtering of each mode in the $i_{th}$ MG, respectively, which can be considered as bandwidth-limited additive white Gaussian noise (AWGN). $I_n(t)$ is the current due to ASE-ASE and signal-ASE beat noises after square-law detection of PD, which can be written as:

$$\begin{aligned} I_n(t) &= 2\mu_{+i}\sum_{m=\pm s}\mathrm{Re}\{E_{\mathrm{OAM}_{+i,m}}(t)n^*_{\mathrm{OAM}_{+i,m}}(t)\} + 2\mu_{-i}\sum_{m=\pm s}\mathrm{Re}\{E_{\mathrm{OAM}_{-i,m}}(t)n^*_{\mathrm{OAM}_{-i,m}}(t)\} \\ &\quad + \mu_{+i}\sum_{m=\pm s}\left|n_{\mathrm{OAM}_{+i,m}}(t)\right|^2 + \mu_{-i}\sum_{m=\pm s}\left|n_{\mathrm{OAM}_{-i,m}}(t)\right|^2 \end{aligned} \tag{5}$$

where $(\bullet)^*$ and $\mathrm{Re}\{\bullet\}$ represent the complex conjugate and the real part, respectively. Here note that, in order to avoid optical interferences between non-orthogonal modes, optical beams from $\mathrm{SMF}_{\pm i}$ output ports of the OAM demux are not directly added together in optical domain and detected by a single PD. From Eq. (4), one can see that if electrical signals from the two received branches of the $i_{th}$ MG are directly combined, the obtained electrical signal is no longer proportional to the optical power, due to the different power response of the two received branches. In addition to the power response difference, there are two other kinds of channel impairments to the two-branch signal reception of the $i_{th}$ MG: 1) the relative delay between the two received branches induced by the differential modal delay between intra-MG

modes, as well as different optical or electrical-path length of the two branches, which will desynchronize the received signals from the two different branches; 2) randomly varying signal-to-noise ratio (SNR) of the two received signals caused by the random power coupling between the $\pm i$ OAM modes, which may deteriorate SNR performance of the desired signal if electrical signals of the two received branches are directly added together with equal weight after equalization (please refer to experimental results in Section 4).

In order to deal with these problems, digital signal processing (DSP) can be employed in the electrical domain, as shown in Fig. 2. For each received branch of the $i_{th}$ MG, electrical signal from the PD is first digitalized by an analog-to-digital convertor (ADC) and then launched to the DSP module. In the DSP module, after resampling and symbol synchronization, signal of each received branch of the $i_{th}$ MG is equalized using either time domain equalization (TDE) or frequency domain equalization (FDE) algorithms [8] to compensate the distortions caused by channel response including differential modal delay, chromatic dispersion, frequency response of the transceiver, etc. In order to maximize the SNR of the received signal regardless of the power fluctuation and the responsivity difference of the two received branches, the two equalized signals of the same MG are combined by using a simple MRC algorithm [23,24]. The MRC output of the $n_{th}$ symbol for each data frame is

$$z(n) = \sum_{l=\pm i} (y_l(n) \times \mathrm{SNR}_l) / \sum_{l=\pm i} \mathrm{SNR}_l \tag{6}$$

where $z(n)$ is the combined signal of the $n_{th}$ symbol used for final symbol decision and demapping to obtain the bit data of the $i_{th}$ MG, $y_l(n)$ with $l = \pm i$ are two equalized signals of the $n_{th}$ symbol, and $\mathrm{SNR}_l$ with $l = \pm i$ are the probed SNRs of the two equalized signals obtained by training symbol and assumed to be quasi-time-invariant within one signal frame. It should be noted that this MRC algorithm can be executed to combine two dependent signals, either in the time domain for pulse-amplitude modulation (PAM) and carrier-less amplitude and phase (CAP) modulation, or in the frequency domain for DMT modulation before final symbol decision at the receiver. Here note that the MRC-based 1×2 receive diversity scheme can also be used for RCF-based LP-MGM system. We emphasize the OAM-MGM system here since the design of our GIRCF is optimized with regard to the OAM modes (details will be found in the next section).

**Table I. RNRM/bit of *M*×*M* MIMO processing and MRC-based 1×*M* SIMO processing.**

**(**$N_{sc}$: number of subcarrier; $N_{FFT}$: number FFT/IFFT size; $r_{os}$: oversampling factor; $N_{MD}$: tap number of modal dispersion equalizer; $N_{bit}$: number of bits per symbols. Here the chromatic dispersion is neglected for short-reach transmission, and $N'_{bit}$ is not equal to $N_{bit}$ assuming the total transmitting powers of these two systems are same.**)**

| Method | Equalizer | RNRM/bit |
|---|---|---|
| Multi-carrier *M*×*M* MIMO processing | TDE | $\frac{4N_{FFT}\log_2(N_{FFT})M + 4N_{FFT}N_{MD}M^2}{N_{sc}N_{bit}M}$ |
| | FDE | $\frac{4N_{FFT}\log_2(N_{FFT})M + 4N_{sc}M^2}{N_{sc}N_{bit}M}$ |
| Multi-carrier based 1×*M* SIMO processing | TDE | $\frac{2N_{FFT}\log_2(N_{FFT})(M+1) + 4N_{FFT}N_{MD}M + 2N_{sc}M}{N_{sc}N'_{bit}}$ |
| | FDE | $\frac{2N_{FFT}\log_2(N_{FFT})(M+1) + 6N_{sc}M}{N_{sc}N'_{bit}}$ |
| Single-carrier *M*×*M* MIMO processing | TDE | $\frac{4N_{MD}M}{N_{bit}/r_{os}}$ |
| | FDE | $4\frac{N_{FFT}\log_2(N_{FFT})M + N_{FFT}M^2}{(N_{FFT}-N_{MD}+1)MN_{bit}/r_{os}}$ |
| Single-carrier MRC-based 1×*M* SIMO processing | TDE | $\frac{4N_{MD}M + 2M}{N'_{bit}/r_{os}}$ |
| | FDE | $4\frac{N_{FFT}\log_2(N_{FFT})M + N_{FFT}M}{(N_{FFT}-N_{MD}+1)N'_{bit}/r_{os}} + \frac{2M}{N'_{bit}}$ |

We also analyze the complexity of the MRC-based receive-diversity single-input multiple-output (SIMO) equalization, compared with that of the MIMO equalization under the same channel condition. As shown in Table I, the complexity per unit capacity of the equalizer can be expressed as the required number of real-valued multiplication (RNRM) per bit, according to the analysis in [8,23–25]. As shown numerators of equations in Table I, the SIMO equalization in the case of $M$ >1 has lower complexity (total complexity, not complexity per unit capacity) than the multiple-input multiple-output (MIMO) equalization with the same modulation (single/multi-carrier) and processing (TDE/FDE) mode and under the same channel condition, although additional complexity of MRC should be considered. On the other hand, according to the Shannon theorem [23], the ratio of capacity between the

MRC-based SIMO and MIMO systems is around $\log_2(M \cdot SNR)/M\log_2(SNR)$ in ideal case regardless of fiber nonlinearity, assuming there is the same total transmitting power in both of the two kinds systems. Here the SNR is that of the MIMO systems. As a result, whether the complexity per unit capacity of the MRC-based SIMO equalization is higher than that of the MIMO equalization or not depends on the system SNR performance and the number of receivers $M$ ($M$=2 in our scheme). Detailed complexity analysis by using paramenters in the experimental demonstrations will be presented in Section 4.

## 3. Fiber design and characterization

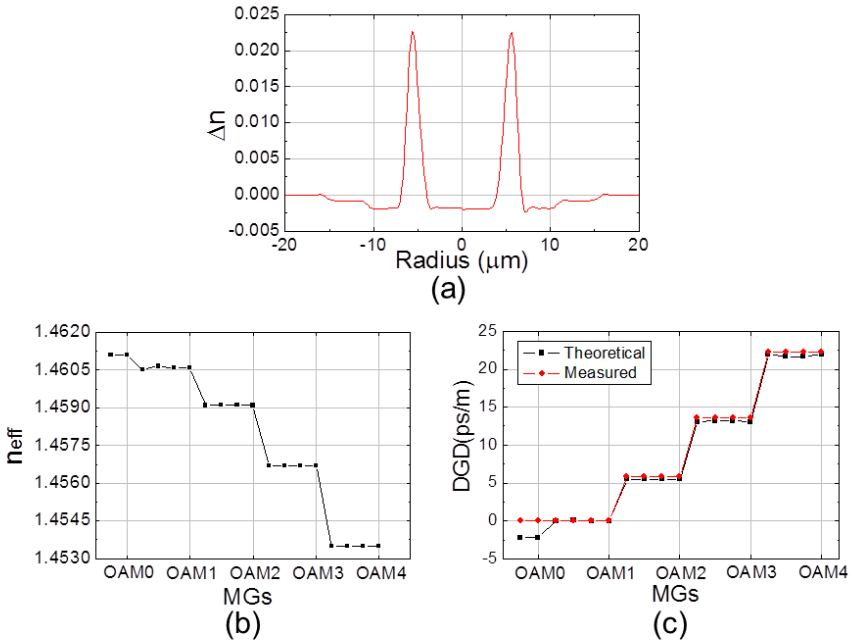


Fig. 3. (a) The refractive index profile of GIRCF; (b) effective indices of MGs in the GIRCF at the wavelength of 1550nm; (c) calculated and measured DGD at the wavelength of 1550 nm.

For proof-of-concept demonstration of the proposed OAM-MGM scheme, a GIRCF supporting mode group order up to $|l|$ = 4 is designed and fabricated. As shown in Fig. 3(a), the GIRCF has a parabolic index profile over the ring-core width to: 1) provide large inter-MG differential effective refractive indices ($\Delta n_{eff}$) to further de-couple the MGs and [see Figs. 3(b)], 2) provide low intra-MG $\Delta n_{eff}$ and thus low differential modal delay between intra-MG modes [26,27] to relieve the frequency-selective fading of IM-DD systems [28] and decrease the complexity of channel equalization (see Table I), 3) soften the radial index gradient thus making the fiber less susceptible to perturbations such as micro-bending [29], and 4) eliminate the spin-orbit-coupling-induced mode purity impairment [27] by removing the step refractive index (RI) interface [30]. It can be seen from Fig. 3(a) that the maximum material RI difference $\Delta n$ is around 0.027, the ring-core radius is around 6.6 μm and the ring-core width is around 3.3 μm. The calculated effective RI of all guided OAM modes and the calculated/measured DGD at the wavelength of 1550 nm are illustrated in Figs. 3(b) and 3(c), respectively. The $\Delta n_{eff}$ and DGD between adjacent MGs increase with the topological order of MGs, and high order MGs ($|l|$ > 1), which will be selected for the demonstration below, promise a higher resistance to inter-MG crosstalk. Here note that there is nearly no difference

of the experimental DGD results between the MGs $|l|=0$ and $|l|=1$ since the two MGs are strongly mixed due to propagation coupling of the 18.4-km GIRCF.

The GIRCF is fabricated by a conventional plasma enhanced chemical vapor deposition (PECVD) process. The measured average propagation attenuation of this fiber is 0.75 dB/km at 1550 nm. This high loss might be caused by the imperfections on two graded index interfaces of the ring core. The sub-system consisting of the GIRCF and the OAM (de)multiplexer (Mux/Demux) devices (i.e., the part in the central dashed box in Fig. 4) is also built to characterize the crosstalk amongst higher order MGs experimentally. The measured results of the 1-km and 18.4-km GIRCF based systems are shown in Table II and III, respectively. It can be deduced that the pure in-fiber mode-coupling induced crosstalk between MGs $|l| = 3$ & 4 over a 17.4-km GIRCF is ~ -9.65 dB in average, while that between MGs $|l| = 2$ & 3 is in average ~ -7.58 dB. Considering the relatively larger inter-MG crosstalk between MGs $|l| = 2$ & 3 in the 18.4-km GIRCF based system, the two high-order MGs $|l| = 3$ and 4 are selected for the OAM-MGM transmission, while three MGs $|l| = 2$, 3 and 4 in the 1-km GIRCF based system are utilized for data transmission demonstration (details will be discussed in next section).

**Table II. The static inter-MG crosstalk (in dB) of entire optical system with 1-km GIRCF.**

| 1-km GIRCF | | Destination MG | | | |
|---|---|---|---|---|---|
| | | $\|l\|=1$ | $\|l\|=2$ | $\|l\|=3$ | $\|l\|=4$ |
| Source MG | $\|l\|=1$ | 0 | -4.43 | -15.03 | -18.57 |
| | $\|l\|=2$ | -5.09 | 0 | -11.26 | -18.04 |
| | $\|l\|=3$ | -17.36 | -11.94 | 0 | -14.05 |
| | $\|l\|=4$ | -20.99 | -17.29 | -13.8 | 0 |

**Table III. The static inter-MG crosstalk (in dB) of entire optical system with 18.4-km GIRCF.**

| 18.4-km GIRCF | | Destination MG | | |
|---|---|---|---|---|
| | | $\|l\|=2$ | $\|l\|=3$ | $\|l\|=4$ |
| Source MG | $\|l\|=2$ | 0 | -5.19 | -7.66 |
| | $\|l\|=3$ | -7.33 | 0 | -8.68 |
| | $\|l\|=4$ | -8.39 | -7.9 | 0 |

## 4. Data transmission demonstration

An IM-DD DMT transmission system is built for the demonstration of the proposed OAM-MGM scheme. The experimental setup is shown in Fig. 4. At the transmitter, the input data bit sequences are firstly mapped into quadrature amplitude modulation (QAM) symbols. After serial-to-parallel (S/P) conversion, the QAM symbols are converted to time domain by 1536-point inverse FFT (IFFT). In order to generate a real-valued DMT signal, the 9th – 264th subcarriers and the 1529th – 1274th subcarriers are used to carry the effective payloads and their complex conjugates, respectively. Then 48-point cyclic prefix (CP) padding, parallel-to-serial (P/S) conversion and hard clipping are performed. For each DMT frame, 11 training symbols are inserted at the beginning of the data frame, which consist of 1 symbol for timing synchronization and 10 symbols for channel estimation and SNR probing. Using an arbitrary waveform generator (AWG) operating at a sample rate of 60-Gsa/s, the electrical DMT signal with an effective bandwidth of 10-GHz is generated. After amplification, the electrical signal

is utilized to modulate an optical carrier at the wavelength of 1550.92 nm though a Mach-Zehnder modulator (MZM) to generate a double-sideband optical signal. Then the generated optical signal is split into three branches, each of which is amplified by an erbium doped fiber amplifier (EDFA) and delayed by a single mode fiber (SMF) with large relative length for data pattern decorrelation.

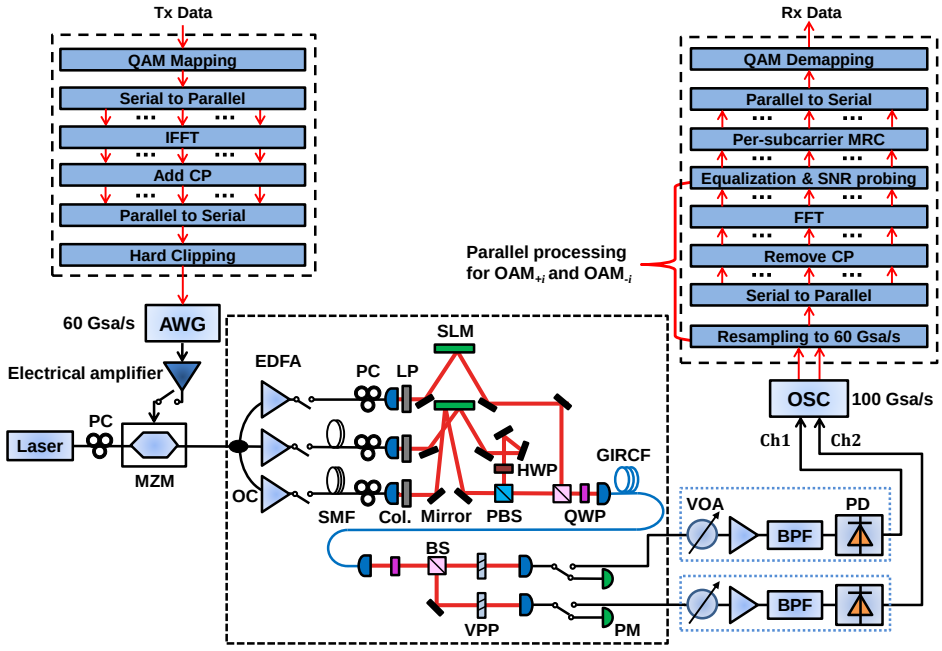


Fig. 4. Experimental setup. AWG: arbitrary waveform generator; PC: polarization controller; MZM: Mach-Zehnder modulator; OC: optical coupler; SMF: single-mode fiber; LP: linear polarizer; SLM: spatial light modulator; PBS: polarizing beam splitter; HWP: half-wave plate; QWP: quarter-wave plate; Col.: collimator; BS: beam splitter; VPP: vortex phase plate; VOA: variable optical attenuator; EDFA: erbium doped fiber amplifier; BPF: band pass filter; PD: photo detector; OSC: oscilloscope. Note that the optical or electrical switches in this figure are utilized to switch between setups for fiber characterization and data transmission.

After being collimated and linearly polarized, the Gaussian beams from the three SMF branches are converted to OAM modes of $l$ = +2, +3 and +4, respectively, using phase-only spatial light modulators (SLMs). Limited by the number of available devices, conversions of OAM modes of $l$ = +3 and +4 are realized by spatially sharing one SLM. By employing a polarization beam splitter (PBS), the two OAM beams of $l$ = +3 and +4 possessing orthogonal linear-polarizations are combined with low loss. Then the two multiplexed OAM beams are combined with the OAM beam of $l$ = +2 by a beam splitter. The generated three coaxial OAM beams are converted into circular polarization states through a quarter-wave plate (QWP) before coupled into the GIRCF, since the eigen OAM states in ring-core fiber are circular polarized. After GIRCF transmission, all output modes from the fiber are converted into linear polarizations and split into two branches. In each branch, the OAM beams are converted to the Gaussian beams by a vortex phase plate (VPP) [31] and then collimated to the SMF pigtail for photo-electric detection. Here it should be noted that the two received branches are used for detection of $\pm i$ OAM modes, respectively, for the reception of the $i_{th}$ MG ($i$ = 2, 3, 4). And only one MG is converted to Gaussian beams at one time due to the device limitation of the VPPs in our lab. The order of VPP should be adjusted when mode conversion for another MG are required.

In each received branch, the optical signal is detected by an optically pre-amplified receiver, which consists of a variable optical attenuator (VOA), an EDFA followed by an optical band-pass filter and a PD. Then the detected electrical signals are digitized and stored by a real time oscilloscope (OSC) with a sampling rate of 100 Gsa/s and finally processed by off-line DSP including resampling, timing synchronization, S/P conversion, FFT, one-tap channel equalization, per-subcarrier MRC [23,24], demapping and error counting.

We performed two sets of MGM transmission over the GIRCFs: transmission of three OAM MGs over a 1-km GIRCF and two OAM MGs over an 18.4-km GIRCF. The back-to-back configuration is also been implemented with a short length of GIRCF (~2-m) between the OAM MUX and DEMUX for system performance comparison, and the BER for each MG are measured and evaluated individually. Figures 5(a)-5(c) show the measured BER results as a function of the received optical power (ROP) (sum of the optical power before the optical pre-amplifiers in each received branch) of the first MGM transmission system, in which three adjacent OAM MGs of $|l|$ = 2, 3 and 4 carrying 10-Gbaud DMT signals are transmitted over a 1-km GIRCF. Here note that the modulation format of the DMT signal carried by OAM MG of $|l|$ = 2 is quadrature phase shift keying (QPSK), while that of the signals carried by other two MGs are 16QAM. The following observations could be made from Figs. 5(a)-5(c): 1) Compared with that in the back-to-back case, power penalties of the MGs $|l|$ = 2, 3 and 4 for single-MG transmission by using MRC technique based on two received branches ($|l|$ = 2, 3 or 4 only, w/ MRC) over the 1-km GIRCF are ~11.5 dB, ~1.1 dB and ~2.6 dB, respectively, at a BER of $3.8\times10^{-3}$. The MG $|l|$ = 2 suffers a much higher power penalty due to relatively stronger inter-MG coupling between MG $|l|$ = 1 and 2 (see Table II). 2) Compared with the single-MG transmission case, power penalties of the MGs $|l|$ = 2, 3 and 4 at a BER of $3.8\times10^{-3}$ for three-MG transmission by using MRC technique ($|l|$ = 2, 3 or 4 w/ MRC) over the 1-km GIRCF are ~1 dB, ~4.5 dB and ~0.7 dB, respectively, which implies that the MG $|l|$ = 3 suffers more crosstalk from the other two MGs, compared with those of the MGs $|l|$ = 2 and 4. 3) Due to the receiver-diversity gain and SNR improvement from MRC, there is a ~2 dB and ~5 dB power budget improvement at a BER of $3.8\times10^{-3}$ for MGs $|l|$ = 2 and 4 by using the MRC technique, respectively, compared with the case based on single-PD detection ($|l| = i$, receive $l = +i$ or $l = -i$, $i$ = 2 and 4). As for the MG $|l|$ = 3, when the receive diversity architecture (two received branches) and MRC technique are utilized, a BER of $3.8\times10^{-3}$ for three-MG transmission over the 1-km GIRCF can be realized at ROP of ~-14 dBm, while the BERs in the case of single-PD detection fail to achieve the 7% hard-decision forward error correction (FEC) limit of $3.8\times10^{-3}$ at a ROP less than -10 dBm. 4) The BER performance of system based on two received branches and equal ratio combining (ERC) technique ($|l|$ = 2, 3 or 4 w/ ERC) is also evaluated for comparison. It can be seen that the there is a similar BER performance for the cases w/ MRC and w/ ERC (the case w/ MRC is slightly better than that of w/ ERC) when the BER performance of $l = +i$ and $-i$ in the case of single-PD detection are approximately same [see Figs. 5(b) and 5(c)]. However, when the BER performance of $l = +i$ and $-i$ have a great difference, there will be an improvement of BER performance for the case w/ MRC compared with that of w/ ERC [see Fig. 5(a)]. Here note that the BER curves in the case of single-PD detection have larger fluctuations, which can be ascribed to severe power fluctuation induced by strong coupling among intra-MG modes. It can be deduced from the results that the system with MRC has much more stable performance compared with that of the system with ERC, considering the random power crosstalk among intra-MG modes. The received constellation diagrams for MG $|l|$ = 3 at ROP of -10.7 dBm after 1-km RCF transmission are shown in Fig. 5(d). Here three receiving schemes are considered, which are single-PD-detection scheme, two-PD-detection scheme w/ ERC and two-PD-detection scheme w/ MRC. It can be seen from the results that the scheme w/ MRC has the best performance among the three cases.

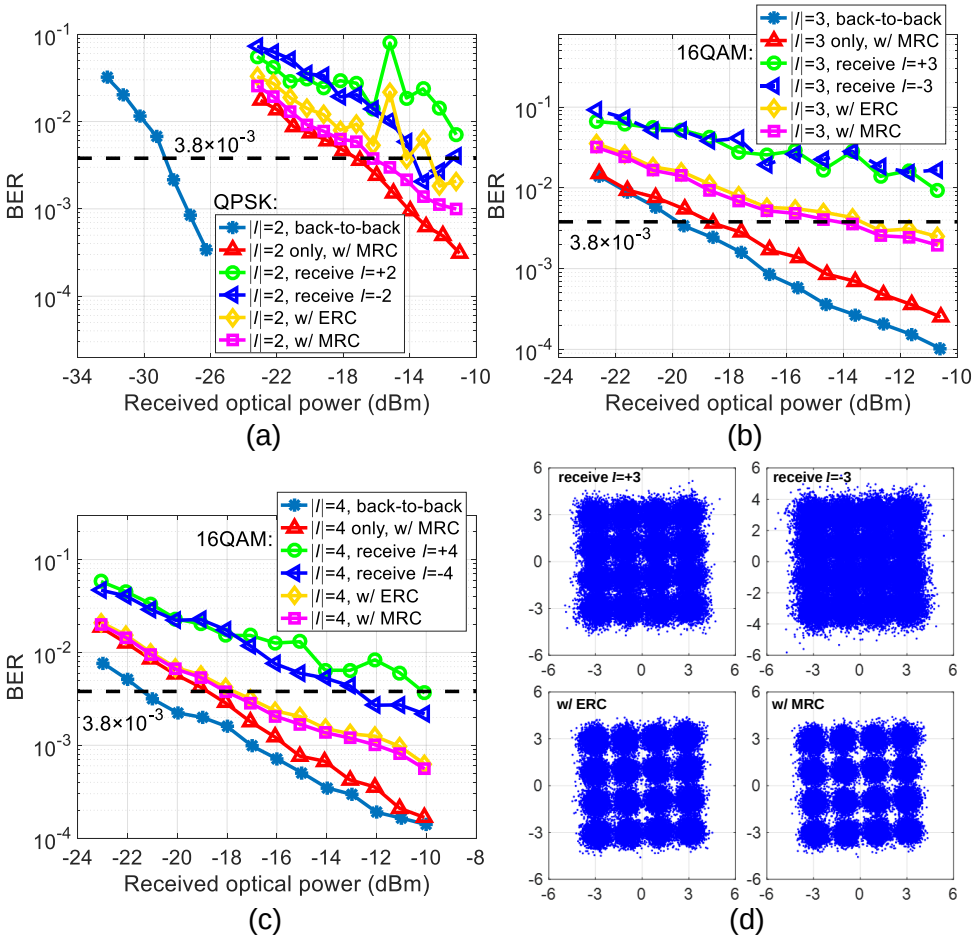


Fig. 5. Measured BER versus ROP for (a) MG $|l|$ = 2, (b) MG $|l|$ = 3, and (c) MG $|l|$ = 4 in the OAM-MGM transmission system over a 1-km GIRCF; (d) received constellation diagrams for MG $|l|$ = 3 at a ROP of -10.7 dBm after 1-km GIRCF transmission.

Figures 6(a) and 6(b) present the measured BER results as a function of the ROP for two mode-group multiplexed transmission over an 18.4-km GIRCF. In this system, two adjacent MGs $|l|$ = 3 and 4 are utilized to transmit DMT signals with QPSK. It can be seen from the results in Figs. 6(a) and 6(b) that: 1) Compared with that in the single-MG transmission case, there are ~2 dB and ~0.9 dB power penalties at a BER of $3.8 \times 10^{-3}$ for MGs $|l|$ = 3 and 4, respectively, in the case of two-MG transmission over the 18.4-km GIRCF. 2) By utilizing the two-PD-detection architecture and MRC technique, the received sensitivity at a BER of $3.8 \times 10^{-3}$ for MGs $|l|$ = 3 and 4 can be improved more than 2 dB and 4 dB, respectively, compared with the single-PD-detection cases. 3) Compared with the two-PD-detection scheme w/ ERC, the scheme with MRC has a better performance for both the MGs $|l|$ = 3 and 4 [see Figs. 6(a) and 6(b)], especially when BER performance of $l = +i$ and $-i$ has a great difference [see Fig. 6(a)].

Figures 6(c) and 6(d) show the SNRs and BERs of individual subcarriers of MG $|l|$ = 3 used for carrying effective payload at a ROP of -20.9 dBm after 18.4-km RCF transmission. One can see that the SNR or BER distributions of two single-PD-detection cases are quite different due to the different received powers resulted random power crosstalk between OAM modes of $l = +i$ and $-i$ and different responses of the two received branches. The SNR in the two-PD-detection system w/ MRC outperforms that w/ ERC, especially when the SNR

performance for $l = +i$ and $-i$ have a great difference, which agree with the results shown in Figs. 6(a) and 6(b). It should be noted that the SNR values of high frequency subcarriers are lower than that of low frequency subcarriers when MRC technique is employed, which results in better BER performance for lower frequency subcarriers. In order to achieve a higher capacity, adaptive bit and power loading algorithm, which can flexibly allocate bits and power for each subcarrier in terms of SNR distribution, could be deployed in future study.

In summary, it can be deduced from the experimental results that the capacity and transmission distance of the OAM-MGM system are mainly limited by the relatively higher attenuation and inter-MG crosstalk of the GIRCF. Future study will focus to improve the fiber design and fabrication process to produce fibers with much lower loss and inter-MG crosstalk.

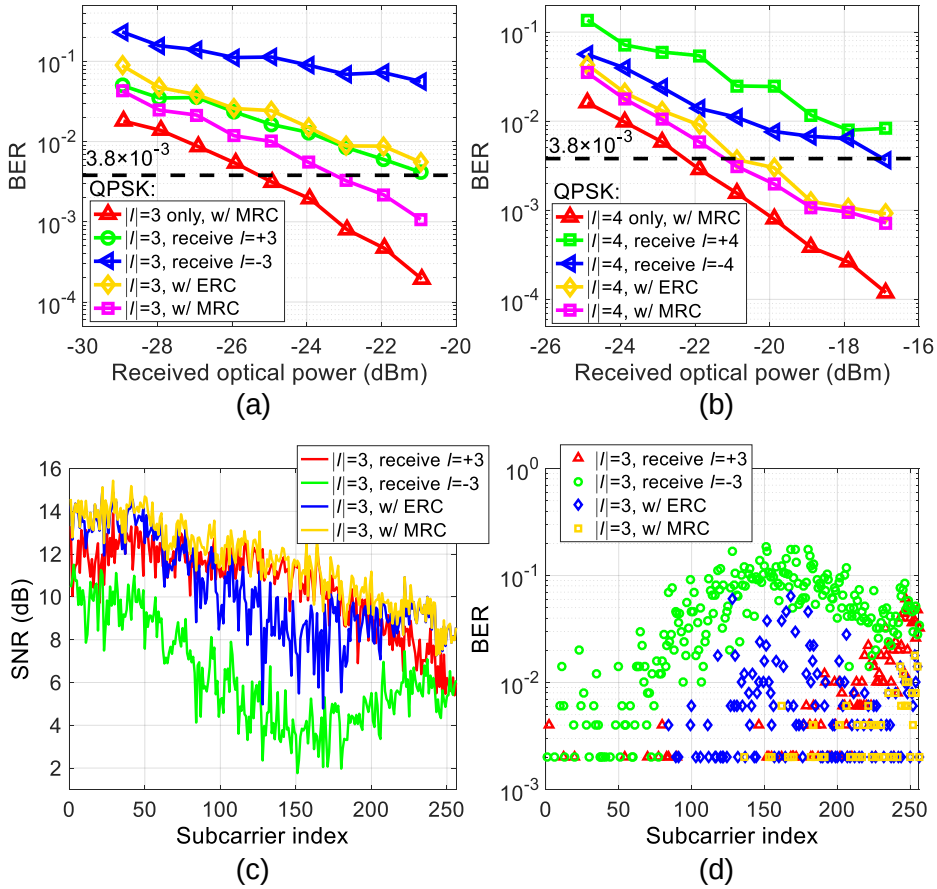


Fig. 6. Measured BER versus ROP for (a) MG $|l|$ = 3 and (b) MG $|l|$ = 4 in the OAM-MGM transmission system over an 18.4-km GIRCF; (c) SNRs and (d) BERs of individual subcarriers of MG $|l|$ = 3 used for carrying effective payload at a ROP of -20.9 dBm after 18.4-km RCF transmission.

In order to evaluate MRC-based SIMO equalization in the demonstrated OAM-MGM systems, Table IV shows the comparison of RNRM per bit for single-input single-output (SISO), MRC-based 1×2 SIMO and 2×2 MIMO equalization by using the parameters in the experiment. Since there is an average of 3-dB SNR improvement of the MRC-based 1×2 SIMO system compared with that of the 2×2 MIMO system with the same transmitting signal power, the value of $N_{bit}$ (bit per symbol) for the 2×2 MIMO system can be deduced according to the specific SNR performance of each mode group and the theoretical SNR thresholds for 7% hard-decision FEC limit of the commonly used modulation formats in the optical fiber

communication systems [23]. Here note that we assume all the intra-group modes are simualtimously detected to avoid the mode partion noise in SISO MGM system and there is no SNR improvement of the MRC-based 1×2 SIMO system compared with it. It can be seen from Table IV that the complexity per unit capacity of the SISO equalization is found to be the lowest. The complexity per unit capacity of MRC-based 1×2 SIMO equalization is slightly higher than that of the 2×2 MIMO equalization for 1-km GIRCF transmission but much lower than that of the 2×2 MIMO equalization for 18.4-km GIRCF transmission in our experimentally demonstrated OAM-MGM systems. It can be seen that the MRC-based 1×2 SIMO equalization performs lower complexity per unit capacity at relatively lower SNR for longer transmission distance.

**Table IV. Complexity analyses of SISO processing, 2×2 MIMO processing and MRC-based 1×2 SIMO processing by using parameters in the experiment.**

<table>
<tr><th>Method</th><th>GIRCF</th><th colspan="3">RNRM/bit/MG</th><th>RNRM/bit</th></tr>
<tr><td rowspan="4">SISO processing (FDE)</td><td rowspan="2">1 km</td><td>MG $|l| = 2$ ($N_{bit} = 2$)</td><td>MG $|l| = 3$ ($N_{bit} = 4$)</td><td>MG $|l| = 4$ ($N_{bit} = 4$)</td><td rowspan="2">78</td></tr>
<tr><td>129</td><td>65</td><td>65</td></tr>
<tr><td rowspan="2">18.4 km</td><td colspan="2">MG $|l| = 3$ ($N_{bit} = 2$)</td><td>MG $|l| = 4$ ($N_{bit} = 2$)</td><td rowspan="2">129</td></tr>
<tr><td colspan="2">129</td><td>129</td></tr>
<tr><td rowspan="4">2×2 MIMO processing (FDE)</td><td rowspan="2">1 km</td><td>MG $|l| = 2$ ($N_{bit} = 1$)</td><td>MG $|l| = 3$ ($N_{bit} = 3$)</td><td>MG $|l| = 4$ ($N_{bit} = 3$)</td><td rowspan="2">112</td></tr>
<tr><td>262</td><td>87</td><td>87</td></tr>
<tr><td rowspan="2">18.4 km</td><td colspan="2">MG $|l| = 3$ ($N_{bit} = 1$)</td><td>MG $|l| = 4$ ($N_{bit} = 1$)</td><td rowspan="2">262</td></tr>
<tr><td colspan="2">262</td><td>262</td></tr>
<tr><td rowspan="4">MRC-based 1×2 SIMO processing (FDE)</td><td rowspan="2">1 km</td><td>MG $|l| = 2$ ($N_{bit} = 2$)</td><td>MG $|l| = 3$ ($N_{bit} = 4$)</td><td>MG $|l| = 4$ ($N_{bit} = 4$)</td><td rowspan="2">118</td></tr>
<tr><td>197</td><td>98</td><td>98</td></tr>
<tr><td rowspan="2">18.4 km</td><td colspan="2">MG $|l| = 3$ ($N_{bit} = 2$)</td><td>MG $|l| = 4$ ($N_{bit} = 2$)</td><td rowspan="2">197</td></tr>
<tr><td colspan="2">197</td><td>197</td></tr>
</table>

## 5. Conclusions

In this paper, we have proposed and experimentally demonstrated an OAM-MGM scheme based on a GIRCF. To suppress the mode partition noise resulting from the random intra-group mode crosstalk, a receive-diversity (1x2 SIMO) architecture has been designed for each MG channel. Moreover, a simple MRC technique has been employed on the receiver side, in order to improve the SNR of the received signals by making use of the diversity gain of receiver. To confirm the feasibility of our proposed OAM-MGM scheme, IM-DD systems transmitting three OAM mode groups with total 100-Gb/s DMT signals over a 1-km GIRCF and two OAM mode groups with total 40-Gb/s DMT signals over an 18.4-km GIRCF have been experimentally demonstrated, respectively. The measured results show that the MRC-based two-PD detection (receive diversity) makes the OAM-MGM systems exhibits best BER performance among the three reception schemes, which are single-PD detection, ERC-based

two-PD detection, as well as MRC-based two-PD detection. The complexity of the MRC-based 1x2 SIMO equalization is also compared with that of the SISO and 2x2 MIMO equalization assuming all of the three kinds of systems have the same transmitting power.

## Funding

SYSU is supported by National Basic Research Program of China (973 Program) (2014CB340000), National Natural Science Foundations of China (61490715, 61505266, 61323001, 11690031, 51403244), Guangdong Natural Science Foundation (2014A030310364, 2016A030313289) and Science and Technology Program of Guangzhou (201707020017). UoB is supported by European Union Horizon 2020 project ROAM.